momentum fluid into the bulk of the flow and an overriding one which returns low momentum fluid to the wall. The major net transfer of low momentum fluid from the wall takes place in a relatively narrow band in the high frequency range near the wall, but further out in the flow it takes place over the full energy-containing range of frequencies.

Frequency scaling of spectra shows that the transition of turbulence to the universal range occurs in the same frequency band throughout the flow. The present findings are also consistent with turbulent heat transfer results.

The authors are indebted to the Australian Institute of Nuclear Science and Engineering for financial support of the work and Dr K. J. Bullock for supervision and encouragement of the authors' theses, which led to the above results.

REFERENCES

Bradshaw, P. 1967 Inactive motion and pressure fluctuations in turbulent boundary layers. *J. Fluid Mech.* **30**, 241–258.

Bremhorst, K. 1969 On the similarity of heat and momentum transfer in fully developed turbulent pipe flow. Ph.D. thesis, University of Queensland, St Lucia.

Bremhorst, K. 1972 The effect of wire length and separation on X-array hot wire anemometer measurements. *Trans. I.E.E.E. Instrum. & Meas.* IM **21**, 244–248.

Bremhorst, K. & Bullock, K. J. 1970 Spectral measurements of temperature and longitudinal velocity fluctuations in fully developed pipe flow. *Int. J. Heat & Mass Transfer*, **13**, 1313–1329.

Bullock, K. J. & Bremhorst, K. 1969 Hot wire anemometer measurements in flows where direction of mean velocity changes during a traverse. *Trans. I.E.E.E. Instrum. & Meas.* IM **18**, 163–166.

Grass, A. J. 1971 Structural features of turbulent flow over smooth and rough boundaries. *J. Fluid Mech.* **50**, 233–255.

Kim, H. T., Kline, S. J. & Reynolds, W. C. 1971 The production of turbulence near a smooth wall in a turbulent boundary layer. *J. Fluid Mech.* **50**, 133–160.

Laufer, J. 1954 The structure of turbulence in fully developed pipe flow. *N.A.C.A. Rep.* no. 1174.

Lawn, C. J. 1971 The determination of the rate of dissipation in turbulent pipe flow. *J. Fluid Mech.* **48**, 477–505, 1971.

Morrison, W. R. B., Bullock, K. J. & Kronauer, R. E. 1971 Experimental evidence of waves in the sublayer. *J. Fluid Mech.* **47**, 639-656.

Narahari Rao, K., Narasimha, R. & Badri Narayanan, M. A. 1971 Bursts in turbulent shear flow. *4th Austr. Conf. Hydraul. & Fluid Mech. Monash University, Melbourne*, pp. 73–78.

Runstadler, P. W., Kline, S. J & Reynolds, W. C. 1963 An experimental investigation of the flow structure of the turbulent boundary layer. *Thermosci. Div. Dept. Mech. Engng., Stanford University Rep.* MD-8.

Walker, T. B. & Bullock, K. J. 1972 Measurement of longitudinal and normal velocity fluctuations by sensing the temperature downstream of a hot wire. *J. Phys.* E, *Sci. Instrum.* **5**, 1173–1178.

J. Fluid Mech. (1973), *vol.* 61, *part* 1, *pp.* 187–198
Printed in Great Britain

The effects of wake splitter plates on the flow past a circular cylinder in the range $10^4 < R < 5 \times 10^4$

By C. J. APELT, G. S. WEST
University of Queensland, Brisbane
AND ALBIN A. SZEWCZYK
University of Notre Dame, Indiana

(Received 3 May 1973)

Experiments were carried out using models having $L/D \leqslant 2$ and the resulting pressure distributions and vortex shedding characteristics are presented. A simple visualization technique which provides explanations of some of the measured results is described. It is concluded that splitter planes reduce the drag markedly by stabilizing the separation points and produce a wake narrower than that for a plain cylinder, raise the base pressure by as much as 50 % and affect the Strouhal number to a lesser degree. Careful measurement techniques have enabled these effects to be presented accurately.

1. Introduction

Experiments reported by a number of authors have shown that the characteristics of the separated wake downstream from a bluff cylinder can be greatly affected when a splitter plate is placed along the centre-line of the wake. When a splitter plate is placed downstream of a circular cylinder in a cross-flow at Reynolds numbers at which a regular vortex street is shed from the plain cylinder, the vortex shedding may be altered or even suppressed and the drag force experienced by the cylinder may be affected. Roshko (1954) reported experiments with splitter plates in the wake of a circular cylinder in a two-dimensional cross-flow at a Reynolds number of $1{\cdot}45 \times 10^4$. He found that a splitter plate of length $5D$ in contact with the cylinder (D is the cylinder diameter) inhibited the periodic vortex formation and caused the pressure drag experienced by the cylinder to be reduced to approximately 63 % of the value for the cylinder alone. A splitter plate of length $1{\cdot}14D$ in contact with the cylinder did not inhibit the vortex formation, but it caused an increase in the base pressure and a reduction in the Strouhal number as compared with the values for the plain cylinder. When the shorter splitter plate was moved downstream leaving a gap between it and the cylinder, Roshko observed a complicated and interesting sequence of changes in the base pressure on the cylinder and in the Strouhal number.

Gerrard (1965) measured the frequency of vortex shedding from a circular cylinder in a cross-flow at a Reynolds number of 2×10^4 with splitter plates of different lengths up to a maximum of $2D$ attached to the cylinder. As the splitter

plate length was increased, the Strouhal number was found to decrease to a minimum for a plate length of approximately D and then to increase as the splitter plate length was increased to $2D$. Apelt & Isaacs (1970) found that very short splitter plates attached to a circular cylinder in a cross-flow at a Reynolds number of $1{\cdot}58 \times 10^4$ caused large reductions in drag. With a splitter plate of length $\frac{1}{8}D$ the pressure drag was reduced to 83 % of the value measured for the plain cylinder. For a splitter plate length of D the pressure drag was reduced to 68 % of the plain-cylinder value, but only relatively small further changes in drag resulted when the splitter plate length was increased in steps up to $8D$.

The results of the experiments referred to demonstrate the complexity of the effects produced by splitter plates in the wake of a circular cylinder, but they do not provide a complete picture of these effects. The experiments described in this paper were designed to provide as complete as possible a description of these phenomena associated with splitter plates, having lengths up to $2D$, attached to a circular cylinder in cross-flows at subcritical Reynolds numbers in the range $10^4 < R < 5 \times 10^4$. The range of Reynolds numbers was chosen since the flow past the plain cylinder in this range is virtually independent of Reynolds number. Detailed measurements have been made of the pressure distribution around the cylinder and of the frequency of vortex shedding from the cylinder and flow visualization studies have been carried out. When taken together these three different sources of information provide a detailed account of the phenomena and enable a coherent explanation of the action of the splitter plates to be made.

2. Experimental work

2.1. *Pressure plotting*

In order to make useful comparisons between the basically similar configurations and flow conditions, it was necessary to aim for a high level of accuracy in the experiments. The regime under investigation was to have a Reynolds number in the vicinity of 10^4, and a cylindrical model 16 mm in diameter achieved this in the existing water tunnel. A simple piezometer tube bank, inclined where necessary, permitted pressures to be measured with the required accuracy over the range of Reynolds numbers from 10^4 to 5×10^4. The water tunnel used is shown in figure 1; it is driven by a variable-speed axial flow propeller and has a working section 330 mm in diameter and 1·6 m long. With the cylindrical model in place this involved an area blockage ratio of 6 % and the water velocities used were well within the capacity of the system.

Preliminary tests established that the velocity profile at the working section was uniform across the core to within 1 %. A simple cylindrical model, spanning the working section and sealed at the tunnel boundary, was used to test the equipment. This model had five pressure holes spaced evenly along a generator between the centre-line and one end, so that, by rotation of the model about its axis and exchanging the positions of its ends, the pressure field round the cylinder at nine spanwise positions could be measured. Except for the pressure hole nearest to the wall, which was in the tunnel boundary layer, nearly identical results were obtained and these agreed well with the well-established results for a plain cylinder (Lienhard 1966).

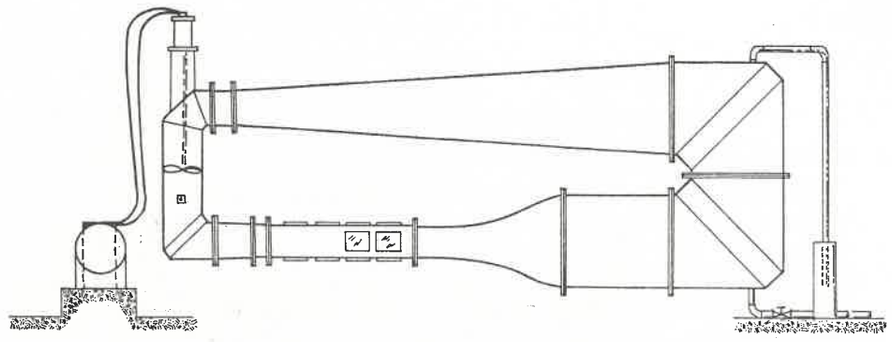

FIGURE 1. Layout of water tunnel.

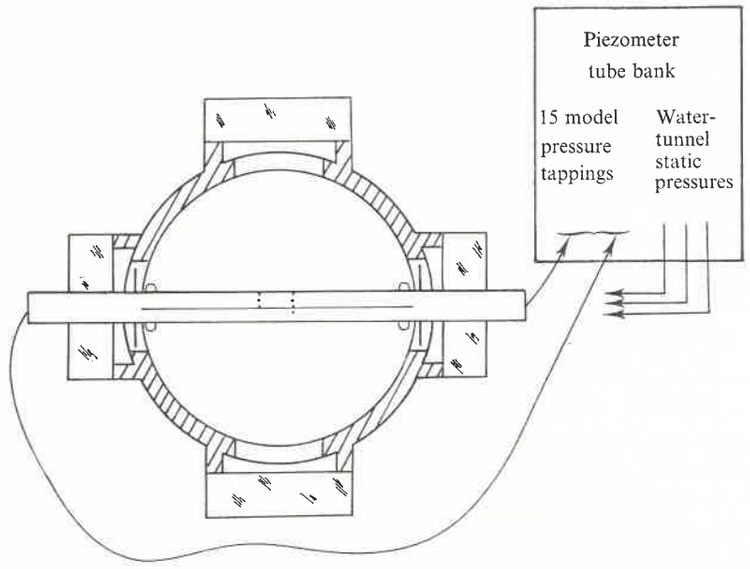

FIGURE 2. Arrangement for pressure plotting.

The main testing programme used a multiple-hole cylindrical model capable of accommodating wake splitter plates of various lengths. The shorter ones ($L/D \leqslant 1$) were 0·5 mm thick; the longer ones were 1·5 mm thick. The whole pressure field was presented simultaneously on the piezometer board, the arrangement being as shown in figure 2.

The following experimental details relating to accuracy and use of the equipment are worth noting.

The model pressure tappings were positioned to within $\frac{1}{4}°$; the slot for the plates required a separate machining operation and was 1° away from its required position at 180°. The pressure holes were originally 2 mm in diameter. To investigate the effects of hole size they were bushed to 0·9 mm; this had no effect on the results, so that 2 mm would have been satisfactory.

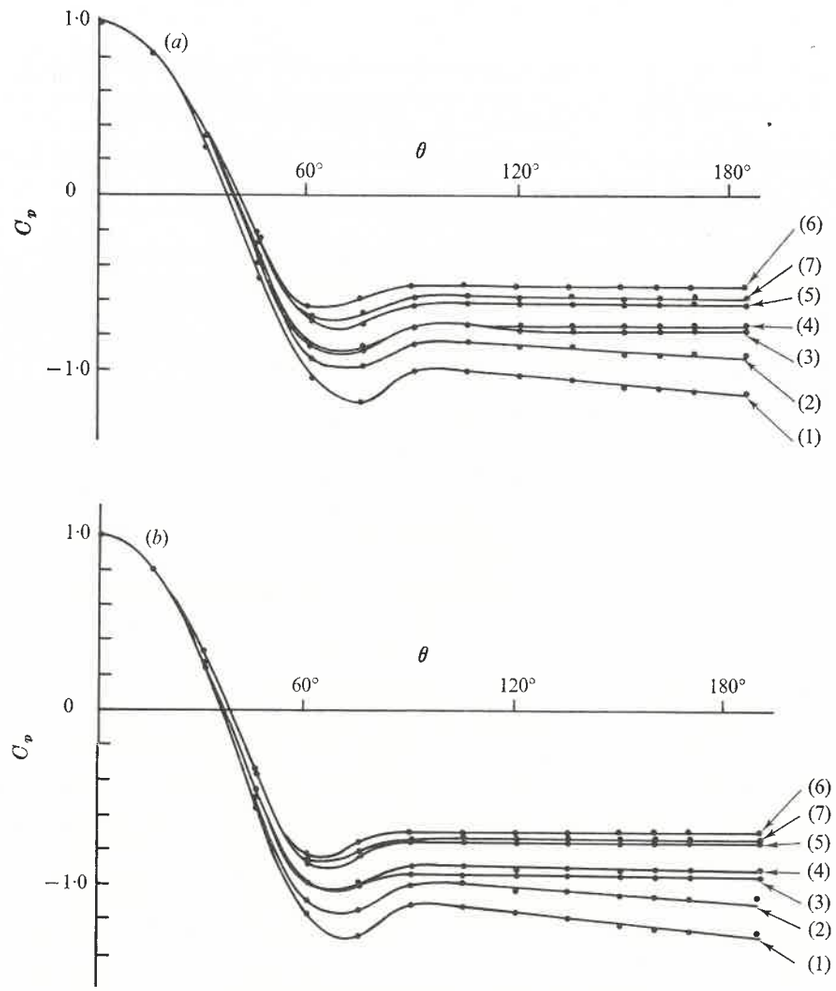

FIGURE 3. C_p *vs.* θ. L/D ratios: (1) 0; (2) $\frac{1}{16}$; (3) $\frac{1}{8}$; (4) $\frac{1}{4}$; (5) $\frac{1}{2}$ and 2; (6) 1; (7) $1\frac{1}{2}$. (*a*) As measured, $R > 2 \times 10^4$. (*b*) Corrected for tunnel blockage.

Orientation of the model is very important; it was rotated until the pressures recorded at $\pm 30°$ were the same. This gave a very fine adjustment. The $\pm 170°$ pressure tappings, though much less sensitive, checked the setting of the splitter plates.

Perfect sealing was necessary where the cylinder passed through the walls of the working section. Without seals the pressure difference between the regions near the observation windows and the wake caused flow into the wake. Neoprene shaft seals were found to be very satisfactory.

The thickness of long splitter plates ($L/D \geqslant 1{\cdot}5$) had to be increased to 1·5 mm to prevent fluttering at high speeds.

Testing was then reduced to the routine of setting up the model, adjusting the flow conditions and recording the piezometer bank readings. Results, in the form C_p *vs.* θ, are shown in figure 3.

2.2. *Wake frequency measurements*

Some confirmatory experiments were undertaken in a wind tunnel on properties of the wake. Primarily these were aimed at measuring vortex frequencies using a hot-wire anemometer. The same equipment is so easily used to plot wake widths and mean and turbulent velocity components that these were also measured for comparison with the visualization studies. The water-tunnel measurements had shown independence of Reynolds number, as discussed below, so that the hot-wire measurements were taken at one Reynolds number only. The wind-tunnel working section was 300 mm square and the model cylinder 2·5 mm in diameter. The Reynolds number used was $2{\cdot}5 \times 10^4$. The anemometer was a Disa 55D05 linearized constant-temperature instrument. The hot-wire anemometer in the wind tunnel was positioned about $4D$ downstream of the model, clear of the wake and the output displayed on an oscilloscope. This was photographed with the graticule superimposed and hence the periodic times obtained. The results, in the form of Strouhal number *vs.* L/D plots, mean velocity contours and turbulence contours, are shown in figure 7 below.

2.3. *Flow visualization*

Visualization studies were carried out in the water tunnel. The pressure plotting model was used with pressure holes at $\pm 30°$ connected to an aniline-dye container. Intense illumination was provided through nearby windows in the working section by 4×500 W quartz–halogen lamps and a high-speed 16 mm camera was mounted near one side window. The opposite side window was painted white with the same finish as the inside of the working section. The camera was run at 500 frames/s for periods of 2–3 s, which gave a sufficient length of film with many repetitions of the flow characteristics. All the visualization runs were made at a Reynolds number of $2{\cdot}2 \times 10^4$ in view of the fact that the phenomena are independent of Reynolds number. Each configuration of cylinder and splitter plate was run twice: once with dye emerging from the $\pm 30°$ holes and once from the 90° hole.

The analysis of the film is described in §3.3.

3. Results: analysis and discussion

3.1. *Pressure plotting*

For each test run the 15 piezometer readings round the cylinder and 3 tunnel static pressure readings along the working section were recorded. Owing to the large number of test runs, the results were processed by computer to give values of the pressure coefficient C_p as a function of position, and the drag coefficient C_d for each Reynolds number. Two sets of these quantities were calculated, the first set being uncorrected for tunnel blockage and the second set corrected

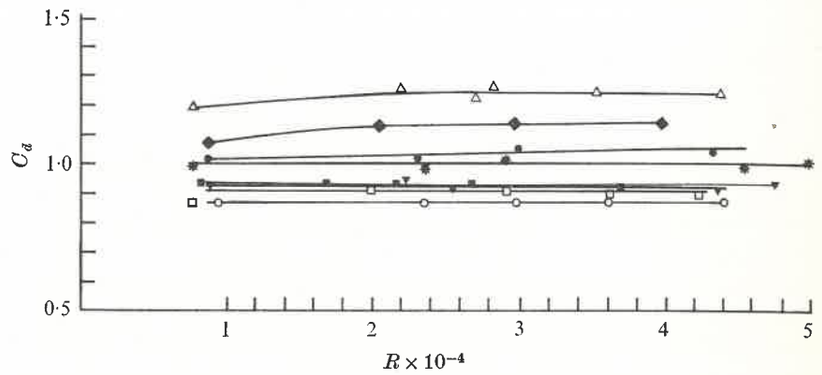

FIGURE 4. C_d *vs.* R. L/D ratios: △, 0; ◆, $\frac{1}{16}$; ●, $\frac{1}{8}$; ✳, $\frac{1}{4}$; ▼, $\frac{1}{2}$; ○, 1; □, $1\frac{1}{2}$; ■, 2.

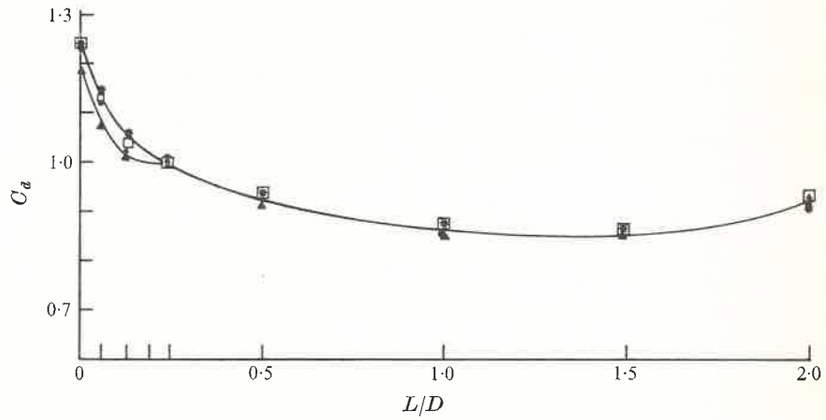

FIGURE 5. C_d *vs.* L/D. Reynolds numbers: ▲, 10^4; ●, 2×10^4; □, 3×10^4; ✳, 4×10^4.

according to Maskell (1963). The area blockage ratio was 6 %. These corrected results are included so that comparisons with other work may be made. However, in this paper uncorrected results are used unless otherwise stated.

The following relationships were used.

(i) $C_p = (p - p_0)/(p_s - p_0)$, where p = pressure, p_s = stagnation pressure, p_0 = static pressure at model position calculated assuming a linear gradient along the working section.

(ii) $C_d = \int C_p \cos d\theta$. This integral was evaluated using Simpson's rule. In this paper C_d represents the pressure drag coefficient.

(iii) The Reynolds number was based on the mean flow velocity and cylinder diameter.

The processed results are set out graphically as C_p *vs.* θ in figures 3 (*a*) and (*b*). Figure 4 shows C_d *vs.* R and demonstrates that, over the range tested, C_d is independent of Reynolds number apart from small variations for plates with $L/D < \frac{1}{4}$. Figures 5 and 6 are alternative presentations of the same information

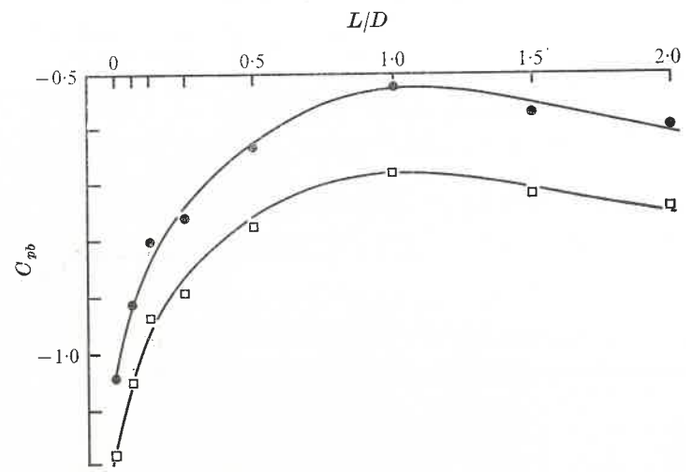

FIGURE 6. C_{pb} *vs.* L/D. ●, corrected for blockage; □, as measured.

and show the drag coefficient and base pressure coefficient plotted against L/D. The large effects produced by very short splitter plates and the presence of a turning point near $L/D = 1$ are evident.

3.2. *Wake characteristics*

Frequencies from the visualization film of events in the water tunnel were obtained by counting the number of frames between repetitions of the same event. This was done for as many cycles as possible and is shown in figure 7 (*a*) as the Strouhal number $S = nD/U$ *vs.* L/D. The results from the hot-wire frequency measurements are also shown on figure 7 (*a*). The two curves are clearly very similar. There is a maximum discrepancy of 5 % at $L/D = \frac{1}{4}$ but the two situations are not the same; the working sections in the water and wind tunnels are of different shape with different turbulence levels and blockage effects. However, the effect of the splitter plate, a slight rise in S up to $L/D = \frac{1}{4}$ followed by a minimum at $L/D = 1$, is well established.

Mean velocity contours of $\overline{u}/U$ were plotted for values of $\frac{1}{4}$, $\frac{1}{2}$, $\frac{3}{4}$ and 1 and a typical set is shown in figure 7 (*b*). The composite diagram of the contours $\overline{u}/U = 1$ for all the configurations tested is shown as figure 8. The reduction of the wake width with increasing L/D is apparent with a very narrow wake at $L/D = 1$.

Figure 7 (*c*) shows contours of turbulent velocity components u'/U.

3.3. *Flow visualization*

The film could conveniently be projected at 16, 8, 4 or 2 frames/s. By this means it was possible to follow events in detail. Tracer dye emerging from the $\pm 30°$ pressure holes in the cylinder was first seen by the camera at $\theta = \pm 90°$, the camera being positioned level with and slightly downstream of the cylinder. The dye was in the form of a solid black line, which shortly afterwards broke up as the separated shear layer became turbulent. Thereafter the formation of vortices around the rear of the cylinder and their departure into the wake could be seen.

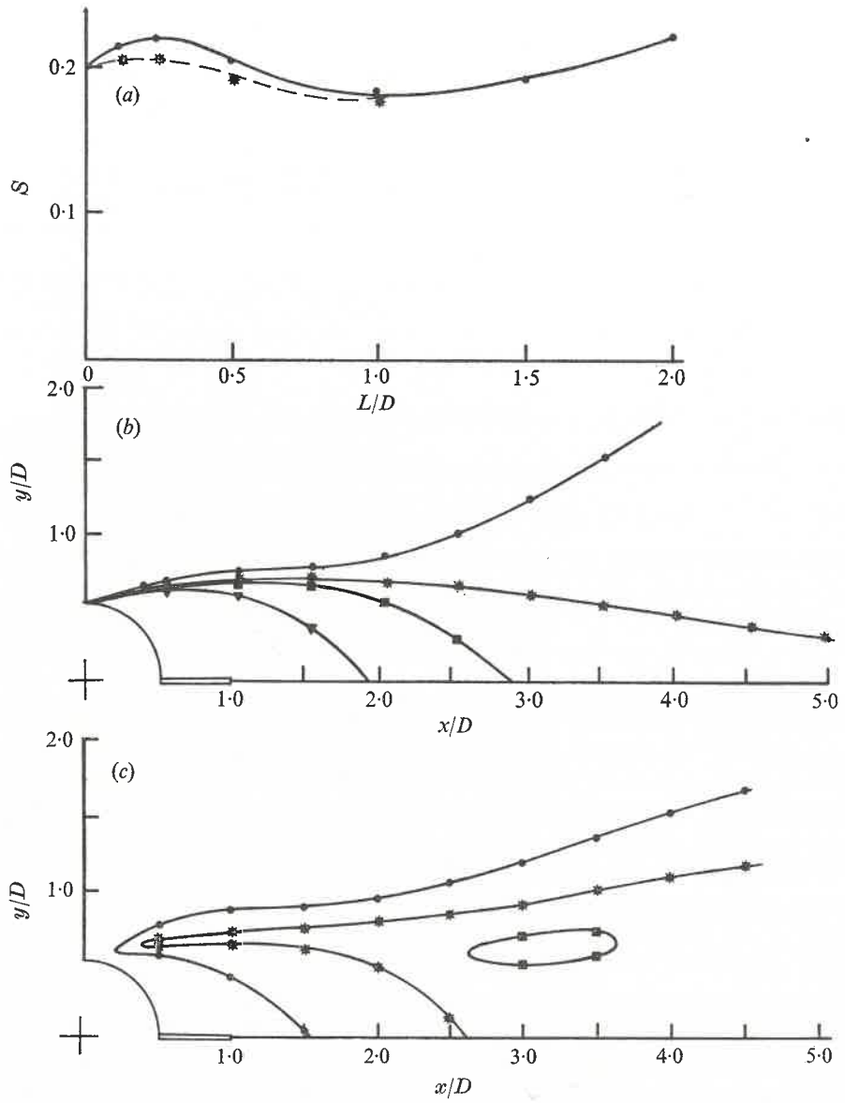

FIGURE 7. (*a*) Strouhal number *vs.* L/D. ●, from film; ✳, from hot-wire anemometer. (*b*) Typical mean velocity contours. $R = 5 \times 10^4$; $L/D = \frac{1}{2}$. $\bar{u}/U$ values: ●, 1; ✳, $\frac{3}{4}$; ■, $\frac{1}{2}$; ▼, $\frac{1}{4}$; (*c*) Typical turbulence contours. $R = 5 \times 10^4$; $L/D = \frac{1}{2}$. u'/U values: ●, 10 %; ✳, 20 %; □, 30 %.

Diagrams have been prepared from the film to illustrate various aspects of the flow. Figure 9 shows envelopes of the wake immediately downstream of the cylinder for all configurations. This was plotted directly from a projection screen, and, owing to the slight obliquity of the camera, is a pictorial representation. However, the following is quite clear.

(i) The wake width is reduced substantially by a very short splitter plate.

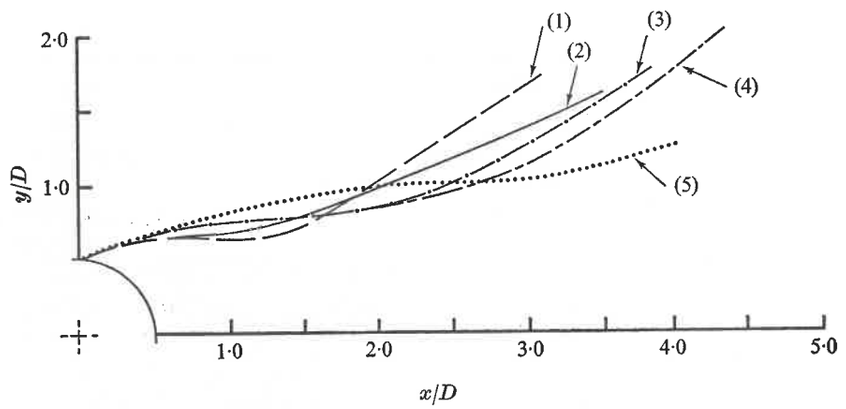

FIGURE 8. Wake envelope from mean velocity contours. $R = 5 \times 10^4$. L/D ratios: (1) 0; (2) $\frac{1}{4}$; (3) $\frac{1}{2}$; (4) $\frac{3}{4}$; (5) 1.

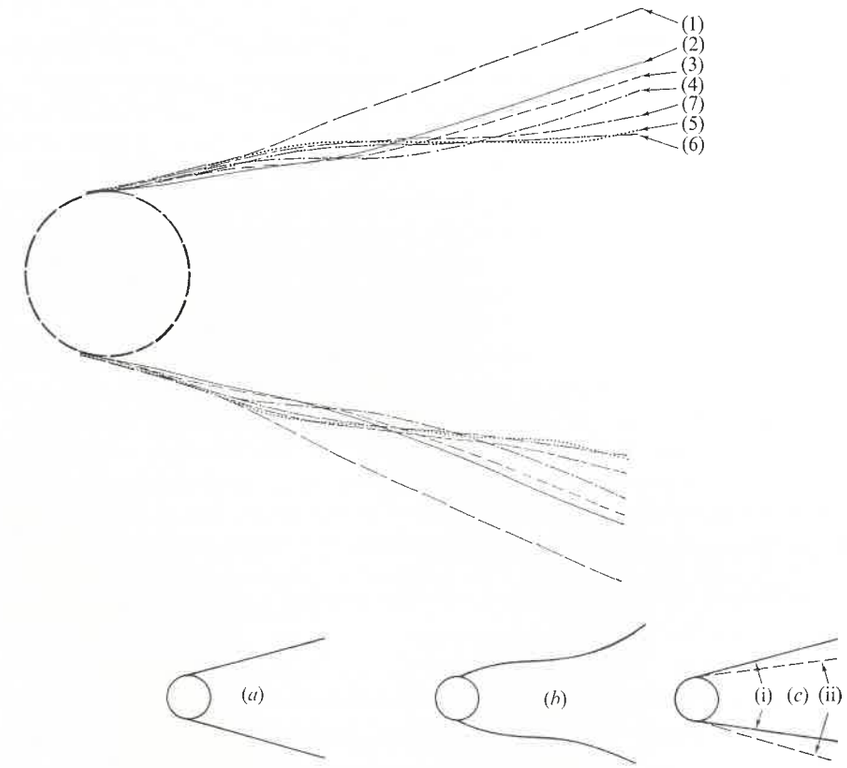

FIGURE 9. Wake envelope from visualization film. L/D ratios: (1) 0; (2) $\frac{1}{8}$; (3) $\frac{1}{4}$; (4) $\frac{1}{2}$; (5) 1; (6) $1\frac{1}{2}$; (7) 2. Inserts: (*a*) 'short' plate, (*b*) 'long' plate, (*c*) effect of movement of separation points.

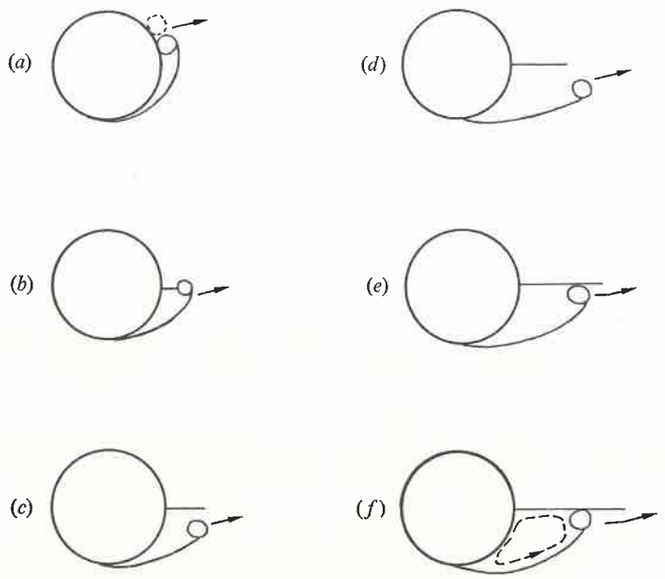

FIGURE 10. Vortex formation. (*a*) Simple cylinder; (*b*) $L/D \leqslant \frac{1}{4}$; (*c*) $L/D = \frac{1}{2}$; (*d*) $L/D = 1$; (*e*) $L/D = 1\frac{1}{2}$; (*f*) $L/D = 2$.

(ii) The wake width is further reduced by longer splitter plates as far as $L/D = 1$–$1{\cdot}5$ but the case $L/D = 2$ shows an increase in wake width.

(iii) Cylinders with very short plates have a simply shaped wake envelope as in figure 9(*a*); increased L/D produces the double curvature of figure 9(*b*). The wake envelope with short plates is produced by movement of the separation points round the cylinder in phase with the vortex shedding. The wake oscillates from position (i) to position (ii) of figure 9(*c*), these positions being approximately 15° apart for a plain cylinder. The shortest plate ($L/D = \frac{1}{8}$) reduced the oscillation of the separation points and the associated oscillation of the wake greatly and at $L/D = \frac{1}{4}$ no oscillation could be detected.

Figure 10 illustrates the vortex formation region for increasing L/D. A plain cylinder has its vortex formation region well forward as in figure 10(*a*). With plates having $L/D = \frac{1}{8}$ and $\frac{1}{4}$ the vortex formed at the edge of the plate as in figure 1(*b*), and the oscillation was progressively reduced as L/D increased. Longer plates cause the vortex to form clear of the plate, as in figure 10(*c*), and then to move towards the plate, roll over the edge as in figure 10(*b*) and wash away into the wake. The double curvature of the wake envelope, figure 9(*b*), for this geometry is clearly due to this. Further increases of L/D reduce the roll-over effect of the departing vortex until at $L/D = 1\frac{1}{2}$ the crossing of the wake centreline is eliminated.

The position of vortex formation moves downstream as L/D increases from 0 to 1, being near the plate trailing edge in each case. Thereafter the formation position remains at essentially the same location with respect to the cylinder. The formation region at $L/D = 1$ is slightly downstream of all the others and, at the same time, is downstream of the plate trailing edge; see figure 10(*d*). It was noted that successive vortices followed each other exactly for $L/D = 1$; in other cases varying degrees of irregularity were observed. These special characteristics of the $L/D = 1$ geometry complement the result that it is the condition with minimum drag and minimum Strouhal number.

By chance, the camera picked up the motion of a very small solid particle in certain cases. The object became involved in the wake formation region for $L/D = \frac{1}{4}$, $\frac{1}{2}$ and 1. With $L/D = \frac{1}{4}$ and $\frac{1}{2}$ it moved off into the wake almost immediately, but with $L/D = 1$ it remained close to the model for a considerable time. It is clear that the region bounded by the plate, the free shear layer and the forming vortex is very quiescent in this case. Unfortunately no solid tracers appeared with the long plates, but dye could be seen to circulate slowly in the corresponding regions for $L/D = 1\frac{1}{2}$ and 2; see figure 10.

3.4. *Discussion*

Reviewing these results leads to a clear division, about $L/D = 1$, between 'short' and 'long' splitter plates. Short plates ($L/D \leqslant 1$) produce a very significant and progressive reduction of drag with increasing L/D, the shortest one tested ($L/D = \frac{1}{16}$) having 91 % of the drag of a plain cylinder and that with $L/D = 1$, the minimum drag condition, 69 % of that of a plain cylinder. These values confirm the results of Apelt & Isaacs (1970) in a wind tunnel; their measured drag reduction of 17 % and 32 % for L/D ratios $\frac{1}{8}$ and 1 compare with 16 % and 31 % in figure 5. The shedding frequencies, however, do not vary monotonically nor do they vary as much; $L/D = \frac{1}{4}$ has a 10 % increase in S and $L/D = 1$ a 10 % decrease from the plain-cylinder values. Gerrard does not observe this rise and fall but there is considerable scatter in his plotted results which could mask it. His value at $L/D = 1$ agrees closely with our figure. It may be significant that $L/D = \frac{1}{4}$ has the highest S and is the geometry for which the separation points first become stabilized but, on the other hand, Bearman's (1965) model, which had stabilized separation points throughout, also showed this rise and fall of S. Longer splitter plates ($L/D > 1$) show increases in both drag and S with L/D over the limited range tested and again the results agree closely with those of Apelt & Isaacs (1970) and Gerrard (1965). The above comparisons are all made between results as measured in different facilities, i.e. not corrected for area blockage. The blockage ratio for the Apelt & Isaacs work was 7·7 %; Gerrard's value is not known; our value was 6 %.

4. Conclusions

(*a*) $C_{\bar{d}}$ is reduced markedly below the plain-cylinder value by a very short splitter plate; for example $L/D = \frac{1}{16}$ effects a 9 % reduction and $L/D = \frac{1}{8}$ a 16 % reduction.

(*b*) $C_{\bar{d}}$ may be reduced by as much as 31 % by an appropriate plate ($L/D = 1$).

(*c*) The maximum change in the base coefficient C_{pb} is at $L/D = 1$; this change is nearly 50 % of the plain-cylinder value.

(*d*) The vortex shedding frequency varies with L/D by $\pm 10\,\%$ (see figure 5*a*) over the range $L/D \leqslant 2$.

(*e*) Around $L/D = 1$, C_d, S and the wake width have minimum values and C_{pb} is a maximum. This should be regarded as the distinction between 'short' and 'long' splitter plates.

(*f*) The action of 'short' plates is to stabilize the separation points progressively and to reduce the wake width with increase of L/D. The trailing edge of the plate provides a fixed formation point for the vortices. 'Long' plates inhibit interaction between the separated shear layers, the vortex forming over the face of the plate, and this results in a rather irregular vortex sheet. However, near the cylinder conditions are much steadier than with short plates.

Acknowledgement is made of support received from the University of Queensland Post-Doctoral Research Fellowship awarded to Professor Szewczyk during 1972.

REFERENCES

Apelt, C. J. & Isaacs, L. T. 1970 Effects of splitter plates placed in the wake of bluff cylinders. *C.A.A.R.C. Symp. on Separated Flows and Wakes, University of Melbourne*.

Bearman, P. W. 1965 Investigation of the flow behind a two-dimensional model with a blunt trailing edge and fitted with splitter plates. *J. Fluid Mech.* **21**, 241.

Gerrard, J. H. 1965 The mechanics of the formation region of vortices behind bluff bodies. *J. Fluid Mech.* **25**, 401.

Lienhard, J. H. 1966 Synopsis of lift, drag, and vortex frequency data for rigid circular cylinders. *Wash. State University Bull.* no. 300.

Maskell, E. C. 1963 A theory of the blockage effects on bluff bodies and stalled wings in a closed wind tunnel. *Aero. Res. Counc. R & M.* no. 3400.

Roshko, A. 1954 On the drag and shedding frequency of two-dimensional bluff bodies. *N.A.C.A. Tech. Note*, no. 3169.

J. Fluid Mech. (1973), *vol.* 61, *part* 1, *pp.* 199–205
Printed in Great Britain

On the existence of multiple Kármán vortex-street modes

By D. WEIHS

Department of Applied Mathematics and Theoretical Physics, University of Cambridge†

(Received 10 April 1973)

An inviscid Kármán-type vortex-shedding model is employed to show that multiple modes of vortex streets are possible, for flow around a given obstacle. This is in confirmation of various experimental observations in recent years, which were challenged by opposing claims that these were due to experimental inaccuracies.

1. Introduction

Several experimental observations of periodic vortex trails behind stationary bodies in two-dimensional flow (Tritton 1959, 1971; Berger 1964) suggest that there are two different possible shedding modes for a certain range of Reynolds numbers. These modes are represented by two vortex streets of different streamwise and lateral spacing appearing alternately under the same experimental conditions, and two separate relationships between the frequency and oncoming flow speed (Reynolds number).

The question of the actual existence of these modes is still rather controversial (Berger & Wille 1972) owing to the work of Gaster (1969, 1971), who concluded that the apparently different modes resulted from non-uniform incoming flow on the obstacle producing the vortex street.

Taneda (1959), who had a unique experimental arrangement permitting observations very far downstream, presented evidence of rather long-lived stable vortex streets suddenly and spontaneously breaking down, and being re-established with larger streamwise and lateral spacing a short distance later. Experiments with decelerated flow (Durgin & Karlsson 1971) and multiple trails (Zdravkovich 1968) also show such behaviour.

This variety of data raises the possibility of alternative vortex–wake developments for a given combination of free-stream flow and obstacle. No theoretical treatment of this phenomenon has been found in the literature, and the purpose of this brief note is to test the possibility of such alternative wake developments occurring, using an inviscid Kármán-type model. The inviscid vortex-shedding approach has given surprisingly good results for different problems, from Kárman's original analysis of shedding from a cylinder to the recent work by Clements (1973) on bluff bodies.

† Present address: Department of Aeronautical Engineering, Technion, Haifa, Israel.